A unique insertion in STARD9's motor domain regulates its stability

Silvia Senese[a], Keith Cheung[a], Yu-Chen Lo[a,b], Ankur A. Gholkar[a], Xiaoyu Xia[a], James A. Wohlschlegel[c,d,e], and Jorge Z. Torres[a,d,e]

[a]Department of Chemistry and Biochemistry, [b]Program in Bioengineering, [c]Department of Biological Chemistry, David Geffen School of Medicine, [d]Jonsson Comprehensive Cancer Center, and [e]Molecular Biology Institute, University of California, Los Angeles, Los Angeles, CA 90095

ABSTRACT **STARD9 is a largely uncharacterized mitotic kinesin and putative cancer target that is critical for regulating pericentriolar material cohesion during bipolar spindle assembly. To begin to understand the mechanisms regulating STARD9 function and their importance to cell division, we took a multidisciplinary approach to define the *cis* and *trans* factors that regulate the stability of the STARD9 motor domain. We show that, unlike the other ~50 mammalian kinesins, STARD9 contains an insertion in loop 12 of its motor domain (MD). Working with the STARD9-MD, we show that it is phosphorylated in mitosis by mitotic kinases that include Plk1. These phosphorylation events are important for targeting a pool of STARD9-MD for ubiquitination by the SCFβ-TrCP ubiquitin ligase and proteasome-dependent degradation. Of interest, overexpression of nonphosphorylatable/nondegradable STARD9-MD mutants leads to spindle assembly defects. Our results with STARD9-MD imply that in vivo the protein levels of full-length STARD9 could be regulated by Plk1 and SCFβ-TrCP to promote proper mitotic spindle assembly.**

Monitoring Editor
Mark J. Solomon
Yale University

Received: Mar 24, 2014
Revised: Nov 21, 2014
Accepted: Dec 2, 2014

INTRODUCTION

During mitosis, kinesins have critical roles in a wide array of processes that contribute to cell division, including spindle assembly, chromosome congression, and cytokinesis (Rath and Kozielski, 2012). To perform their functions, mitotic kinesins require ATP hydrolysis. This feature makes them amenable to small-molecule inhibition with ATP-competitive or allosteric inhibitors. Not surprisingly, mitotic kinesins have received considerable attention as potential targets in the treatment of proliferative diseases such as cancer (Rath and Kozielski, 2012). Indeed, clinical trials are underway to test the efficacy of mitotic kinesin inhibitors in the treatment of cancer (Rath and Kozielski, 2012). Recently, we identified steroidogenic acute regulatory protein–related lipid transfer (START) domain containing 9 (STARD9), a member of the kinesin-3 family of molecular motors, as an important factor for stabilization of the pericentriolar material (PCM) under microtubule-mediated tension in early mitosis (Torres *et al.*, 2011). Depletion of STARD9 by small interfering RNA (siRNA) treatment leads to PCM fragmentation, multipolar spindles, failure to congress chromosomes, mitotic arrest, spindle assembly checkpoint activation, and a faster apoptotic cell death than current antimitotic drug treatments, indicating that STARD9 is a potential target for therapeutic intervention (Torres *et al.*, 2011; Torres, 2012). However, little is known about the molecular basis of STARD9's mechanism of action and the regulatory mechanisms modulating its activity.

Although there are many mechanisms that regulate kinesin activity (including autoinhibition, perturbation of the kinesin–microtubule interaction, and sequestration of kinesins to specific cellular compartments), phosphorylation of mitotic kinesins by mitotic kinases (such as Plk1, Cdk1, and Aurora A/B) has emerged as a sensitive switch to modulate kinesin activity in a spatial-temporal manner (Andrews *et al.*, 2004; Cahu *et al.*, 2008; Jang *et al.*, 2009; Verhey and Hammond, 2009). For example, Plk1 phosphorylates the kinesin-13 motor MCAK during mitosis to promote its microtubule-depolymerization activity, which is necessary for proper chromosome segregation (Zhang *et al.*, 2011). Plk1 also phosphorylates factors important for mitotic progression (Emi1 and Bora), centrosome

This article was published online ahead of print in MBoC in Press (http://www.molbiolcell.org/cgi/doi/10.1091/mbc.E14-03-0829) on December 10, 2014.
Address correspondence to: Jorge Z. Torres (torres@chem.ucla.edu).
Abbreviations used: LAP, localization and affinity purification; MD, motor domain; PBD, polo-box domain; SCF, Skp/Cullin/F-box; STARD9, steroidogenic acute regulatory protein–related lipid transfer (START) domain containing 9.

maturation (pericentrin), PCM cohesion (Kizuna), microtubule nucleation and dynamics (Nlp and stathmin), and bipolar spindle assembly (Budde *et al.*, 2001; Casenghi *et al.*, 2003; Barr *et al.*, 2004; Hansen *et al.*, 2004; Oshimori *et al.*, 2006; Seki *et al.*, 2008a; Lee and Rhee, 2011). The mechanism of Plk1 substrate phosphorylation typically involves the binding of its carboxyl-terminal polo-box domains (PBDs) to serine-[phosphoserine/phosphothreonine] (S_pS, S_pT) motifs within substrates before its amino-terminal kinase domain can transfer phosphoryl groups onto substrates (Elia *et al.*, 2003; Lowery *et al.*, 2007).

In addition to phosphorylation, cell cycle progression and cell division are largely controlled by two multisubunit ubiquitin ligases, anaphase-promoting complex/cyclosome (APC/C) and Skp1/Cul1/F-box protein–β-TrCP (SCFβ-TrCP), which ubiquitinate and target cell cycle regulators for degradation by the proteasome (Cardozo and Pagano, 2004; Frescas and Pagano, 2008; Barford, 2011). In the case of the SCFβ-TrCP, β-TrCP (an SCF substrate adaptor) binds to canonical DSGXXS motifs found in IκBα, claspin, Emi1, and other substrates only when both of the motif's serine residues are phosphorylated, which facilitates their ubiquitination and targeting for degradation (Winston *et al.*, 1999; Margottin-Goguet *et al.*, 2003; Mailand *et al.*, 2006; Frescas and Pagano, 2008). In addition, β-TrCP can bind to noncanonical sites, including the DSGXXT motif within Bora (Seki *et al.*, 2008a). Although several kinases can phosphorylate serine/threonine residues within canonical and noncanonical β-TrCP recognition motifs, G2/M substrates are predominantly phosphorylated by Plk1, including claspin, Bora, and Emi1 (Margottin-Goguet *et al.*, 2003; Mailand *et al.*, 2006; Seki *et al.*, 2008a). On the other hand, the APC/C degrades several kinesins during mitotic exit, including the kinesin-5 motors Kip1p and Cin8p (*Saccharomyces cerevisiae*), the orphan kinesin motor AtKINUa (*Arabidopsis thaliana*), and kinesin-10 Xkid (*Xenopus laevis*; Funabiki and Murray, 2000; Gordon and Roof, 2001; Hildebrandt and Hoyt, 2001; Malcos and Cyr, 2011). However, to our knowledge, none of the ~50 human kinesins have been reported to be regulated by the SCFβ-TrCP.

Here we applied a multidisciplinary approach to understand the *cis* and *trans* factors that regulate the protein levels of the STARD9 motor domain (MD). Molecular modeling of the STARD9-MD identified a conserved insertion in loop 12, which harbored putative Plk1 binding sites (SS motifs) and an extended DSGXXSS β-TrCP-binding motif. Of interest, this insertion is heavily phosphorylated by mitotic kinases that include Plk1, which enables STARD9-MD's ubiquitination by the SCFβ-TrCP ubiquitin ligase and its bulk degradation by the proteasome. Overexpression of nonphosphorylatable/nondegradable STARD9 motor domain mutants led to spindle assembly defects, mitotic arrest, and reduced cell viability. Our analysis of the STARD9-MD implies that STARD9 protein levels are regulated through posttranslational modifications and that this may be important for proper cell division.

RESULTS

The STARD9 motor domain harbors a unique insertion with putative regulatory sequences

The large size of STARD9 (~517 kDa) greatly complicates its expression and molecular manipulation (Figure 1A). To better understand the function of STARD9 in cell division, we sought to characterize its kinesin motor domain, which plays a critical role in STARD9's function (Torres *et al.*, 2011). To do this, we first modeled the structure of the STARD9-MD (amino acids 1–391) based on the KIF1A motor domain (with which it shares 48% sequence identity) crystal structure (Protein Data Bank [PDB] ID 1IA0) using the homology modeling program Modeller (Sali and Blundell, 1993; Figure 1B and Supplemental Figure S1). The STARD9-MD structure was evaluated with the structural analysis verification server and by Ramachandran plot, which showed that 92.1% of the residues were in the most favored region and 0% of the residues were in disallowed regions (Ramachandran *et al.*, 1963; Luthy *et al.*, 1992; Colovos and Yeates, 1993; Laskowski *et al.*, 1993; Shen and Sali, 2006; Figure 1B and Supplemental Figures S1 and S2). Structure alignment of STARD9-MD with KIF1A-MD showed strong structural conservation, with the exception of a few extended loops (L7, L11, and L12) in STARD9 (Pettersen *et al.*, 2004; Figure 1B and Supplemental Figure S3). Based on modeling, the STARD9 L12 was predicted to be unstructured and could potential adopt multiple conformations (one conformation is depicted in Figure 1B).

Of interest, we identified a 26–amino acid insertion in L12 that contained putative Plk1 polo-box domain (PBD) binding sites (SS motifs) and a DSGXXS β-TrCP (SCFβ-TrCP ubiquitin ligase substrate adapter) binding motif, indicating that STARD9 may be regulated through posttranslational modifications such as phosphorylation and ubiquitination (Figure 1C). The L12 insertion, the Plk1-PBD binding sites, and the β-TrCP-binding motif were highly conserved among all identified STARD9 mammalian orthologues (Figure 1D). A survey of the full-length STARD9 protein indicated that the DSGXXS β-TrCP-binding motif within the motor domain was the only one present within the entire protein, which was also true for all STARD9 mammalian orthologues. In addition, the STARD9 DSGILS motif matched the canonical DSGXXS β-TrCP-binding motif found in β-TrCP substrates such as IκBα, claspin, and Emi1 (Winston *et al.*, 1999; Margottin-Goguet *et al.*, 2003; Mailand *et al.*, 2006; Frescas and Pagano, 2008; Figure 1E). Consistent with a role of the ubiquitin-proteasome system in regulating STARD9 function, previous analyses showed that transient overexpression of STARD9-MD led to modest increase in PCM fragmentation and multipolar spindle formation (Torres *et al.*, 2011).

Cell cycle regulation of STARD9-MD protein levels

To determine whether STARD9-MD protein levels were cell cycle regulated by the ubiquitin-proteasome system, we generated a doxycycline-inducible localization and affinity purification (LAP = enhanced green fluorescent protein [EGFP]–tobacco etch virus–S-peptide)–tagged STARD9-MD HeLa stable cell line that expresses STARD9-MD from a single specific locus within the genome to monitor STARD9-MD protein levels throughout the cell cycle (Torres *et al.*, 2009). Indeed, STARD9-MD levels remained high in G1/S and mitotic cells in the presence of the proteasome inhibitor MG132 (a representative immunoblot is shown in Figure 2A). However, STARD9-MD protein levels decreased in mitotic cells in the absence of MG132 (a representative immunoblot is shown in Figure 2A). In addition, a higher–molecular weight band corresponding to a modified form of STARD9-MD was apparent in mitotic cells (Figure 2A, arrows). To determine whether this modification was specific for mitosis, we synchronized cells in G1/S and released them into the cell cycle in the presence of nocodazole. Cells were then harvested every 2 h and lysed, and protein samples were analyzed by immunoblot analyses (Figure 2B). STARD9-MD was unmodified in G1/S and became modified at ~8 h postrelease during mitotic entry (a representative immunoblot is shown in Figure 2B, arrows). To further verify that STARD9-MD levels were decreasing during mitosis, cells synchronized in early mitosis with nocodazole were released, and samples were collected every hour and analyzed by immunoblotting. STARD9-MD protein levels decreased as the cells were released from early mitosis and exited mitosis and increased again as

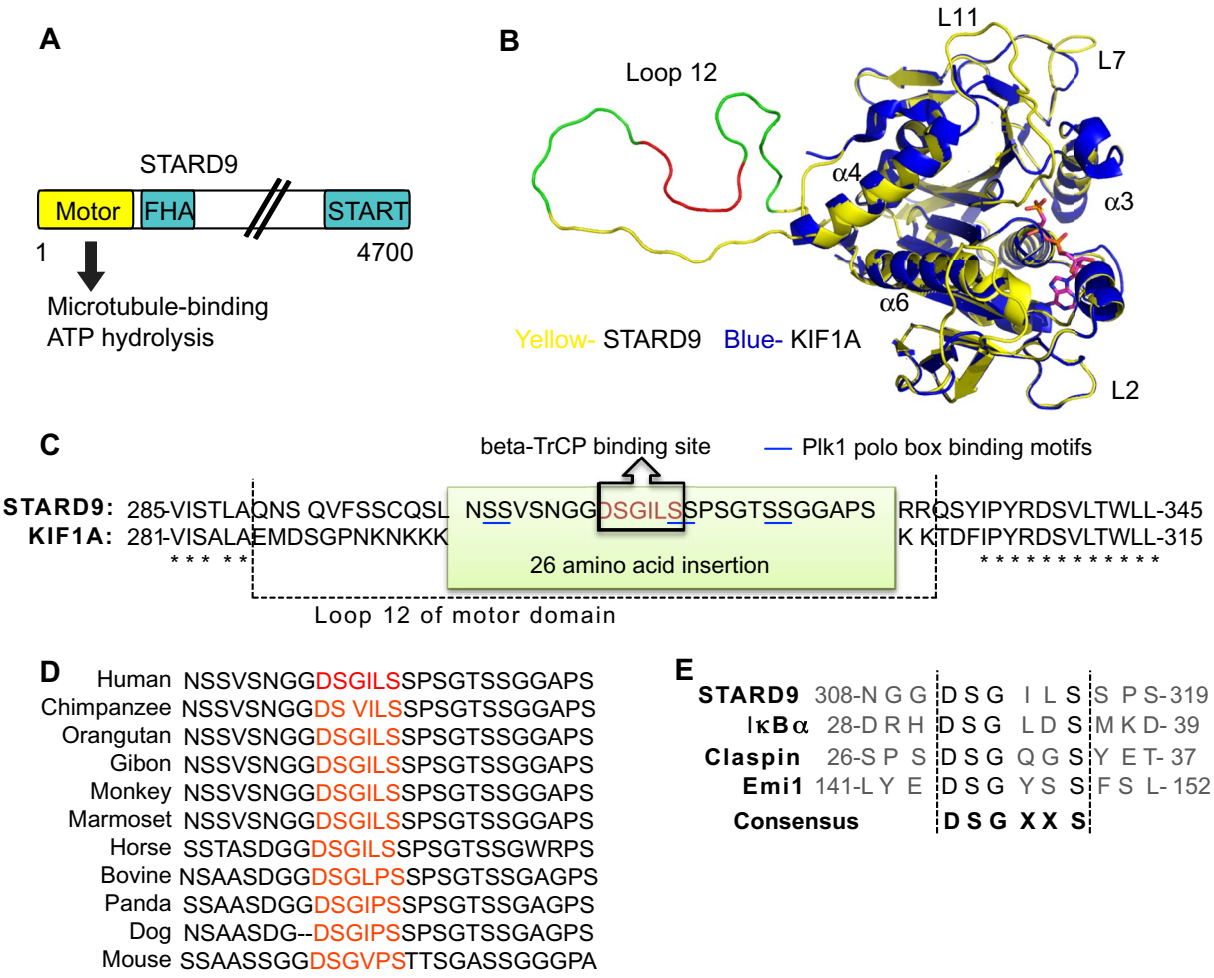

FIGURE 1: The STARD9 motor domain loop 12 harbors a unique insertion with Plk1 and β-TrCP binding sites. (A) Schematic of the STARD9 modular domain composition. (B) Molecular modeling of the STARD9 motor domain using the KIF1A motor domain crystal structure (PDB ID 1IA0). Note that loops 7, 11, and 12 are extended. (C) Compared with KIF1A, STARD9 contains a 26–amino acid insertion in loop 12 with putative Plk1 polo-box domain–binding motifs (SS) and a β-TrCP DSGXXS–binding motif. (D) The 26–amino acid insertion and DSGXXS motif are highly conserved among STARD9 mammalian orthologues. (E) Alignment of STARD9, IκBα, claspin, and Emi1 β-TrCP DSGXXS–binding motifs and consensus.

the cells entered G1 (Figure 2C). Similar to the experiments with living cells, recombinant glutathione *S*-transferase (GST)–STARD9-MD remained unmodified when incubated with G1/S extracts and became modified and degraded when incubated with mitotic extracts (Figure 2D, arrows). These results indicated that STARD9-MD is modified posttranslationally during mitosis and contained the minimal sequences required for STARD9-MD's cell cycle– and proteasome-dependent degradation.

Proteomic analysis of the STARD9 motor domain

Because STARD9-MD contained several potential phosphorylation sites, we asked whether the modified form of STARD9-MD was due to phosphorylation. Extracts were prepared from G1/S or mitotic cells expressing STARD9-MD and were subjected to λ phosphatase treatment (Figure 3A). Consistent with our previous results, STARD9-MD was only modified in mitosis and not G1/S (Figure 3A). Of interest, the modified form of STARD9-MD was absent when extracts were treated with λ phosphatase (Figure 3A), indicating that the modified form of STARD9-MD was due to phosphorylation. Consistently, when recombinant GST-STARD9-MD was incubated with mitotic extracts it became modified, and the addition of λ phosphatase reversed this modification (Figure 3B). To further define the phosphorylation events that were likely regulating STARD9-MD stability, we took an unbiased proteomic approach to map the STARD9-MD amino acids that were phosphorylated in mitosis. The LAP-STARD9-MD HeLa stable cell line was used to express and tandem affinity purify STARD9-MD (Torres *et al.*, 2009). Purifications were carried out from G1/S and mitotic cell extracts in the presence of phosphatase, protease, deubiquitinase, and proteasome inhibitors to preserve PTMs and prevent protein degradation. Eluates from these purifications were separated by gel chromatography, and the band corresponding to the phosphorylated form of STARD9-MD (present only in the mitotic purification) was excised and analyzed by mass spectrometry (Figure 3C). STARD9-MD peptides were then inspected for mass spectra shifts indicative of phosphorylation (ST: +79.9663 Da). Surprisingly, we identified 10 phosphorylation sites within STARD9-MD, and nine of 10 phosphorylation sites mapped to the L12 insertion (Figure 3, D and E). Nine of the

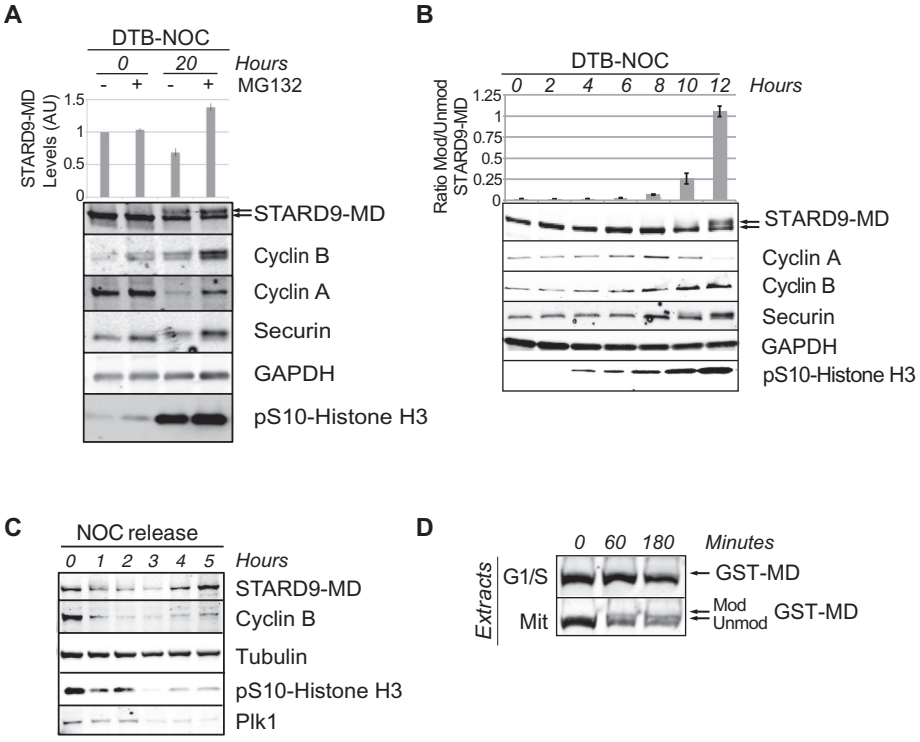

FIGURE 2: The STARD9 motor domain is modified and degraded in mitosis. (A) The LAP-tagged STARD9-MD cell line was double thymidine blocked (DTB; 0 h) and released into the cell cycle in the presence of nocodazole (NOC; 20 h) ± MG132. Extracts were immunoblotted with indicated antibodies, and the levels of STARD9-MD were quantified (arbitrary units [AU]) for each condition. Data represent the average ± SD of three independent experiments. (B) Same as in A, except that no MG132 was added, and protein extracts were prepared at the indicated time points and analyzed by immunoblotting with the indicated antibodies. The ratio of modified/unmodified STARD9-MD was quantified for each condition as indicated. Data represent the average ± SD of three independent experiments. (C) The LAP-tagged STARD9-MD cell line was synchronized in early mitosis with nocodazole for 16 h and released into fresh medium. Samples were collected each hour and analyzed by immunoblotting with the indicated antibodies. Plk1 was used as a mitotic marker (degraded in early G1 phase). Note that STARD9-MD protein levels decreased during mitosis when Plk1 was present. (D) Recombinant STARD9-MD (GST-MD) was incubated with G1/S or mitotic extracts, and the appearance of the modified form of GST-MD was monitored by immunoblot analysis.

phosphorylation sites were on serines (serines 304, 305, 307, 312, 316, 317, 319, 328, and 332) and one was on threonine 321, with serines 305 and 317 being the most abundantly phosphorylated (Figure 3, D and E, and Supplemental Figure S4). Of interest, serines 312 and 316 within the DSGXXS motif were phosphorylated, indicating that a DpSGXXpS phosphodegron could be regulating STARD9-MD protein levels (Figure 3, D and E, and Supplemental Figure S4). In addition, two putative Plk1-PBD binding sites, S316:S317 (SpSP canonical) and S304:S305 (SpSV noncanonical), were also phosphorylated (Figure 3, D and E, and Supplemental Figure S4).

Phosphorylation of the STARD9-MD L12 insertion regulates STARD9-MD protein stability

Owing to the large number of phosphorylation sites within the STARD9-MD, we focused on serine residues that spanned the putative Plk1-PBD SpS binding sites (S304:S305 and S316:S317) and the β-TrCP-binding DpSGXXpS motif (S312 and S316) that were found phosphorylated in mitosis (Figure 3, C–E, and Supplemental Figure S4). To analyze the importance of phosphorylating these serines, we generated LAP-tagged STARD9-MD stable cell lines that had each site mutated to an alanine (S304A, S305A, S312A, S316A, and S317A, all mutants integrated at the same loci within the genome). In addition, we generated double-mutant (S312/316A) and triple-mutant (S312/316/317A) stable cell lines. Next we analyzed the importance of phosphorylation for STARD9-MD protein stability. Wild-type and serine mutant cell lines were synchronized in G1/S, released, and treated with nocodazole for 12 or 20 h and the stability of STARD9-MD monitored by immunoblot analysis. Whereas wild type, S304A, and S316A were degraded by 20 h, S305A, S312A, S317A, the double mutant, and the triple mutant remained stabilized (Figure 4A). Consistently, protein half-life experiments (in which cells were synchronized in early mitosis with nocodazole and released into the presence of cycloheximide, with samples collected every hour and analyzed by immunoblotting) showed that S305A, S312A, and S317A STARD9-MD mutants had a longer half-life than wild-type STARD9-MD (Figure 4B). These results indicated that the phosphorylation of S305, S312, and S317 played critical roles in the degradation of STARD9-MD. β-TrCP is also known to bind and ubiquitinate proteins with a modified consensus that includes one or two additional amino acids between the two phosphoserines—example p105 (DpSGVETpS) and CDC25A (DpSGFCLDpS; Busino *et al.*, 2003; Lang *et al.*, 2003). Because S312 and S317 were phosphorylated and played a role in the degradation of STARD9-MD, we asked whether the β-TrCP substrate-binding site could accommodate the extended consensus STARD9-MD phosphodegron (DpSGILSpS). Indeed, similar to a previous analysis of p105 and CDC25A, molecular modeling indicated that the β-TrCP substrate-binding site within the WD40 domain accommodated the DpSGILSpS peptide, with the extended hydrophobic part of the peptide moving deeper into the pocket (Kanarek *et al.*, 2010; Figure 4C and Supplemental Figure S5).

Phosphorylation of STARD9-MD by Plk1 is required for its degradation

Given that STARD9-MD harbored Plkl binding sites that were phosphorylated in mitosis (S304pS305 and S316pS317; Figure 3, C–E), we asked whether Plk1 bound to STARD9-MD and was able to phosphorylate it. LAP-tagged STARD9-MD wild type or S317A was immunoprecipitated from G1/S or mitotic cells, and eluates were immunoblotted for Plk1. Indeed, endogenous Plk1 bound preferentially to the mitotic phosphorylated STARD9-MD in comparison to the G1/S nonphosphorylated STARD9-MD (Figure 5A). Furthermore, endogenous Plk1 was unable to bind the nondegradable/nonphosphorylated S317A STARD9-MD mutant (Figure 5A). Consistently, overexpressed hemagglutinin (HA)-Plk1-KD (kinase-dead form, binds to substrates but does not phosphorylate them) coimmunoprecipitated with STARD9-MD from mitotic cells (Supplemental Figure S6). The interaction between Plk1 and

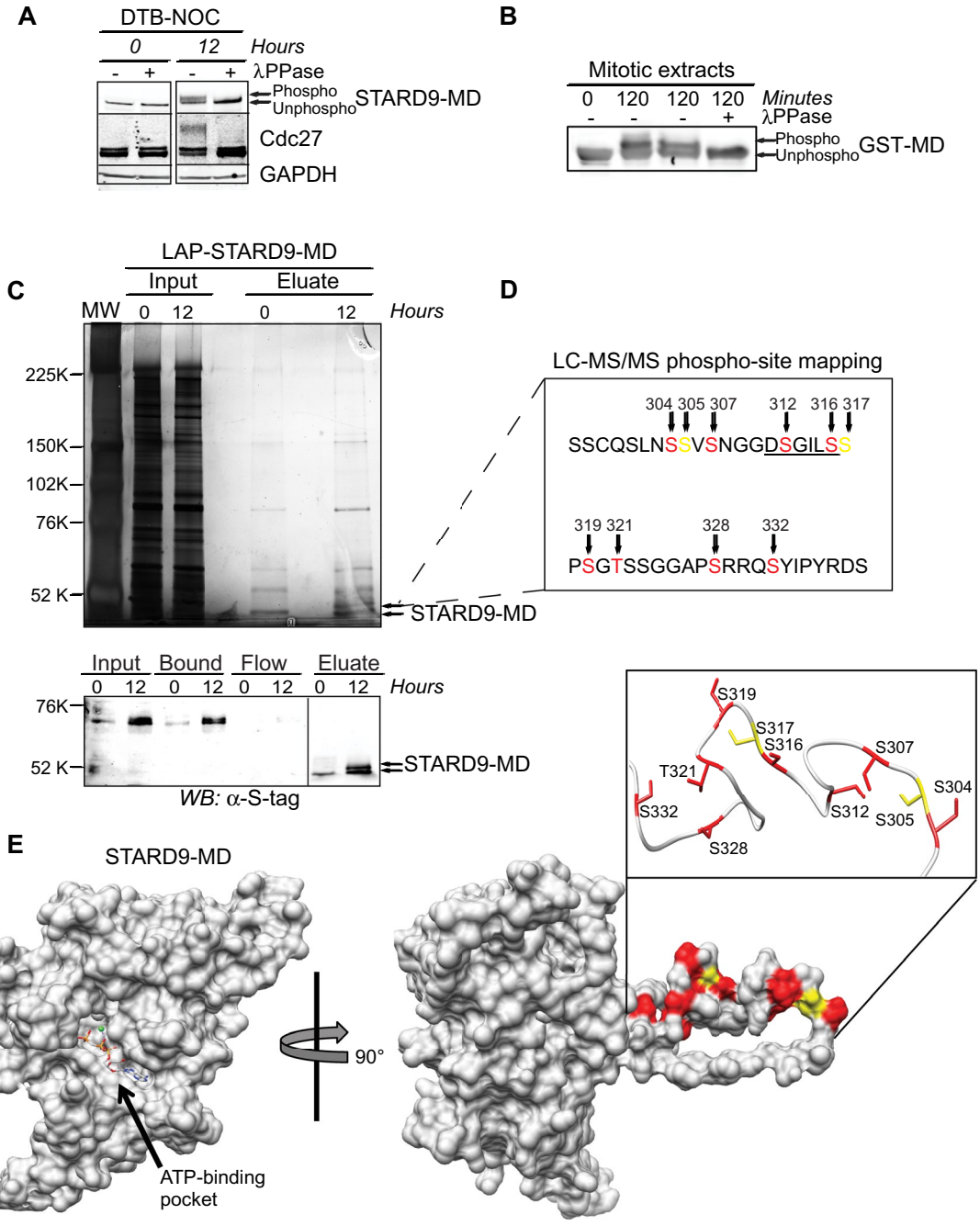

FIGURE 3: Proteomic analysis of the STARD9 motor domain. (A) STARD9-MD was purified from G1/S (thymidine, 0 h) or mitotic (nocodazole, 12 h) extracts and either treated or not treated with λ phosphatase and analyzed by immunoblot analysis with the indicated antibodies. (B) Recombinant GST-STARD9-MD was incubated with mitotic extracts in the presence or absence of λ phosphatase, and the appearance of the modified form of GST-STARD9-MD was monitored by immunoblot analysis. (C) Tandem affinity purification of LAP-STARD9-MD from G1/S (thymidine, 0 h) or mitotic (nocodazole, 12 h) HeLa cell extracts. Eluates were separated by SDS–PAGE, and protein bands were visualized by silver staining the gel. Immunoblot analysis of these samples was used to verify the identity of STARD9-MD throughout the purification process. The phosphorylated STARD9-MD band present only in mitotic purifications was excised and analyzed by mass spectrometry to map phosphorylation sites. (D) Identified STARD9-MD phosphorylation sites are highlighted with arrows and their amino acid position. Red amino acids were phosphorylated, and yellow amino acids were found to be the most abundantly phosphorylated. (E) The phosphorylation sites were mapped onto the STARD9-MD modeled structure. Nine of 10 phosphorylation sites mapped to the 26–amino acid insertion in the flexible loop 12, and one was outside this region.

phosphorylated STARD9-MD was also assessed by in vitro binding assays in which in vitro translated HA-Plk1 or HA-Plk1-KD both immunoprecipitated preferentially with recombinant phosphorylated (incubated with mitotic extracts) GST-STARD9-MD compared with nonphosphorylated (not incubated with mitotic extracts) STARD9-MD and control GST (Supplemental Figure S6). These

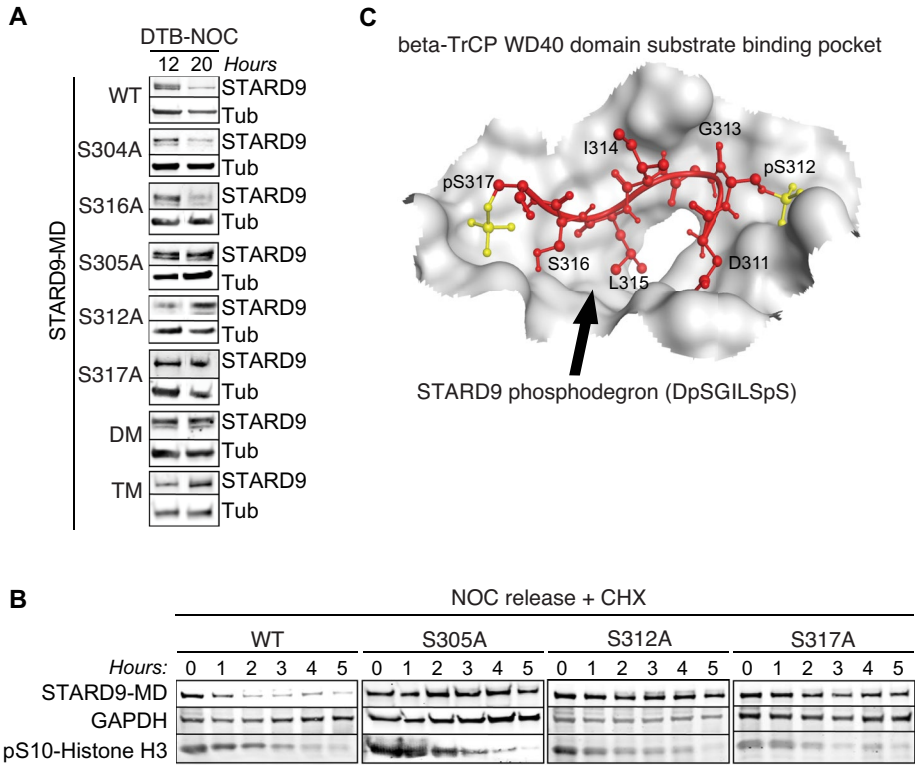

FIGURE 4: Phosphorylation at serines 305, 312, and 317 regulates STARD9-MD protein stability. (A) HeLa stable cell lines expressing STARD9-MD wild type, serine-to-alanine single mutants (S304A, S305A, S312A, S316A, and S317A), double mutants (S312/316A), and triple mutants (S312/316/317) were arrested in G1/S and released into the cell cycle in the presence of nocodazole for 12 or 20 h. Extracts from these time points were immunoblotted to monitor the levels of STARD9-MD and tubulin. (B) HeLa stable cell lines expressing STARD9-MD wild type and serine-to-alanine single mutants (S305A, S312A, and S317A) were arrested in early mitosis with nocodazole for 16 h and treated with cycloheximide during the release. Samples were collected each hour and analyzed by immunoblotting to monitor the levels of STARD9-MD. (C) Molecular modeling of the interaction between β-TrCP and the STARD9-MD extended phosphodegron (DpSGILSpS) peptide.

results indicated that Plk1 was binding to phosphorylated STARD9-MD. Next we asked whether Plk1 could directly phosphorylate STARD9-MD. In vitro phosphorylation assays were carried out with recombinant wild type or serine-to-alanine STARD9-MD mutants and [γ-^{32}P]ATP in the presence or absence of recombinant Plk1. The transfer of the [γ-^{32}P]phosphate group onto STARD9-MD was then monitored by Western blot and radiometric analyses. In this assay, Plk1 was able to phosphorylate wild type and S304A, S305A, S316A, and S317A single mutants, although S304A, S305A, and S316A had a minimal reduction in phosphorylation compared with wild type. However, only minimal phosphorylation was observed with the S312A single mutant and the double and triple mutants that also contained the S312A mutation (Figure 5B). These results indicated that Plk1 was phosphorylating S312 and that phosphorylation at other serines was likely due to other mitotic kinases. Finally, we asked whether Plk1 regulated STARD9-MD protein levels in vivo. Treatment of cells with the Plk1 inhibitor BI2536 or GSK461364 led to the stabilization of STARD9-MD in mitosis (a representative immunoblot is shown in Figure 5C). Consistently, depletion of Plk1 in LAP-tagged STARD9-MD wild-type cells, which had been synchronized in early mitosis with nocodazole and released into the cell cycle, inhibited the degradation of STARD9-MD (Figure 5D). To assess further whether Plk1 phosphorylation was regulating the degradation of STARD9-MD, we transfected the LAP-tagged STARD9-MD cell line with HA-Plk1 or HA-Plk1-KD overexpression vectors and monitored the stability of STARD9-MD by immunoblot analysis during release from early mitosis. Overexpression of HA-Plk1 led to a decrease in STARD9-MD protein levels, whereas overexpression of HA-Plk1-KD (binds and inhibits phosphorylation of substrates) led to a stabilization of STARD9-MD (Figure 5E). On the other hand, the depletion of Plk1 (Figure 5D) or overexpression of Plk1 or Plk1-KD (Figure 5E) did not change the protein levels of S312A STARD9-MD mutant, indicating that phosphorylation of S312 played an important role in the modulation of STARD9-MD protein levels. Together these results indicated that Plk1 was able to bind to phosphorylated STARD9-MD and was responsible for phosphorylating it at serine 312 and that this phosphorylation event was critical for regulating STARD9-MD protein stability.

β-TrCP binds to STARD9-MD and is required for its degradation

The binding of β-TrCP to canonical ($D_pSG(2X)_pS$) and extended phosphodegrons ($D_pSG(3X)_pS$ or $D_pSG(4X)_pS$) is critical for SCFβ-TrCP substrate ubiquitination and degradation (Margottin *et al.*, 1998; Busino *et al.*, 2003; Lang *et al.*, 2003). Our mass spectrometry and mutagenesis data indicated that serines 312 and 317 within the STARD9-MD DpSGXXSpS motif were phosphorylated in mitosis and required for STARD9-MD degradation. Thus we asked whether β-TrCP was able to interact with STARD9-MD, by performing coimmunoprecipitation assays. In these assays, phosphorylated or nonphosphorylated GST-STARD9-MD was obtained after incubation with or without M-phase–arrested cell extracts (Figure 6A). The two forms of GST-STARD9-MD were incubated with HA-β-TrCP or HA-β-TrCPΔF (dominant-negative mutant is able to bind substrates but not ubiquitinate them) and immunoprecipitated. The association of HA-β-TrCP or HA-β-TrCPΔF with STARD9-MD was then analyzed by immunoblot analysis. HA-β-TrCP and HA-β-TrCPΔF both immunoprecipitated preferentially with phosphorylated GST-STARD9-MD compared with nonphosphorylated GST-STARD9-MD and control GST (Figure 6B and Supplemental Figure S7). Conversely, β-TrCP did not immunoprecipitate with the nonphosphorylatable/nondegradable S317A STARD9-MD mutant (Figure 6, C and D). To determine the importance of β-TrCP in regulating the levels of STARD9-MD in mitosis, we overexpressed HA-β-TrCP or HA-β-TrCPΔF in cells and analyzed their effect on STARD9-MD protein levels during their release from nocodazole. Overexpression of HA-β-TrCP led to a slight reduction in the levels of STARD9-MD compared with control (CTRL) transfections during mitosis (Figure 6E). In contrast, overexpression of HA-β-TrCPΔF led to the stabilization of STARD9-MD in mitosis (Figure 6E). Accordingly, siRNA-mediated RNA interference targeting endogenous β-TrCP resulted in the stabilization of STARD9-MD (Figure 6, F and G) during mitosis. These results indicated that β-TrCP bound to

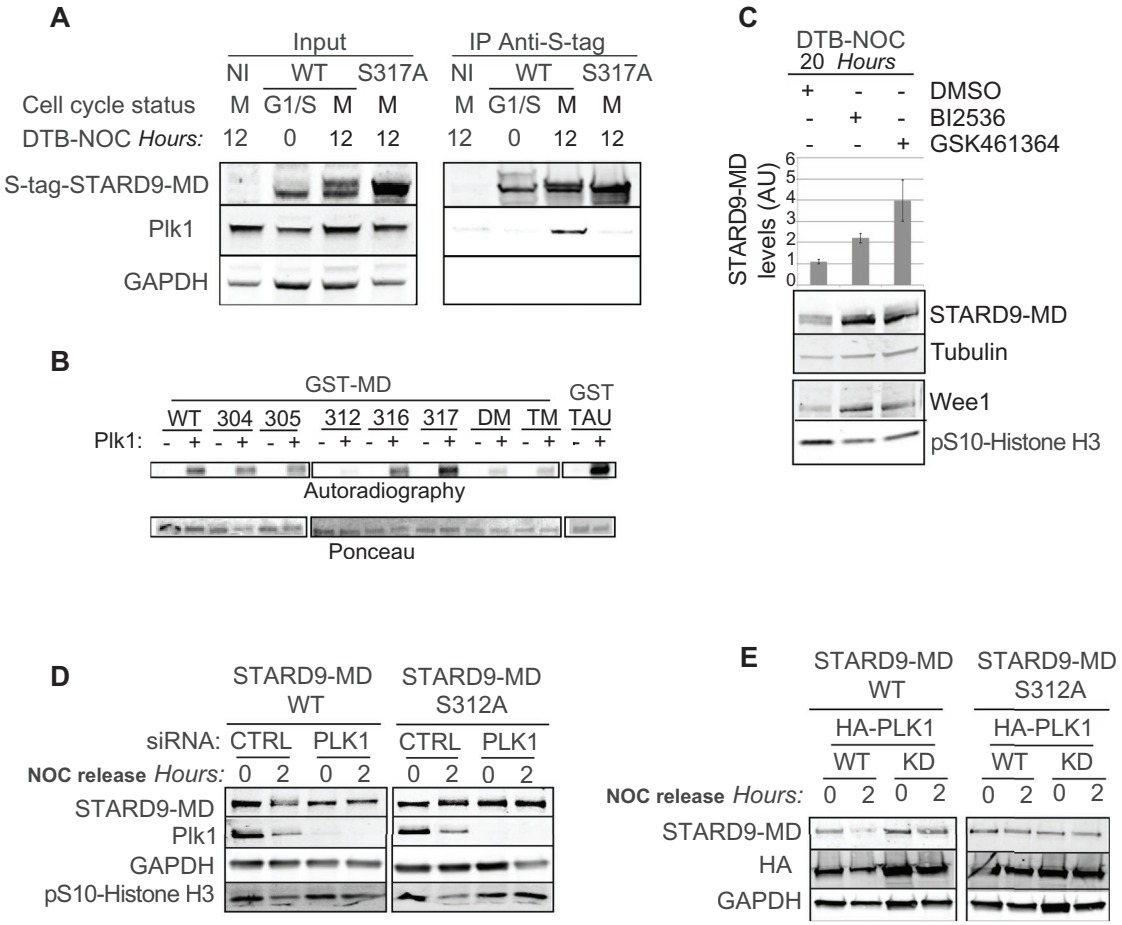

FIGURE 5: Plk1 binds to STARD9-MD, phosphorylates it at serine 312, and regulates its degradation. (A) Immunoprecipitation of LAP-tagged STARD9-MD wild type and S317A mutant from G1/S or mitotic extracts. Eluates were immunoblotted for the indicated proteins. Note that Plk1 only coimmunoprecipitates with mitotic phosphorylated wild-type STARD9-MD and not the nonphosphorylated S317A STARD9-MD mutant. NI indicates the noninduced control. (B) Plk1 phosphorylates STARD9-MD at serine 312. In vitro phosphorylation assays were carried out with recombinant wild type or serine-to-alanine mutant STARD9-MD. The transfer of the [γ-^{32}P]phosphate group onto STARD9-MD was monitored by Western blot and radiometric analyses. (C) Plk1 regulates STARD9-MD protein levels in vivo. The LAP-tagged STARD9-MD cell line was synchronized in G1/S and released into nocodazole-containing media in the presence or absence of BI2536 or GSK461364 Plk1 inhibitors, mitotic cells were harvested 20 h postrelease, protein extracts were analyzed by immunoblotting for the indicated proteins, and the levels of STARD9-MD were quantified for each condition. Data represent the average ± SD of three independent experiments. (D) siRNA knockdown of endogenous Plk1 protein in LAP-tagged STARD9-MD wild-type and S312A mutant cell lines. Cells were synchronized in early mitosis with nocodazole for 16 h and released, and samples were collected at the indicated time points and immunoblotted with the indicated antibodies. CTRL indicates control siRNA. (E) The LAP-tagged STARD9-MD wild-type and S312A cell lines were transfected with HA-Plk1 or HA-Plk1-KD overexpression vectors, cells were arrested in mitosis with nocodazole for 16 h and released into fresh medium, and extracts were prepared at the indicated time points and immunoblotted with the indicated antibodies.

phosphorylated STARD9-MD and that SCFβ-TrCP was involved in the degradation of STARD9-MD in a cell cycle–dependent manner. To further test this, we asked whether STARD9-MD was an SCFβ-TrCP substrate in an in vitro reconstituted ubiquitination assay (Laney and Hochstrasser, 2011). For these assays, recombinant GST-STARD9-MD was incubated with an ATP-regeneration system, ubiquitin, an E1 ubiquitin- activating enzyme, an E2 ubiquitin-conjugating enzyme, and the SCFβ-TrCP (recombinant Skp1, ±Cul1, ±β-TrCP and Roc1). Reactions were incubated at 30°C for 120 min, and ubiquitination products were resolved by SDS–PAGE and immunoblotted with anti-ubiquitin and anti-GST antibodies. We observed polyubiquitin STARD9-MD as a ladder of increasing molecular weight bands that was largely reduced in the absence of Cul1 or β-TrCP (Figure 6H). In these assays, Emi1 served as a positive control and GFP as a negative control. Together these results indicated that β-TrCP preferentially binds to phosphorylated STARD9-MD and that STARD9-MD is an SCFβ-TrCP substrate.

Increased STARD9-MD protein levels lead to PCM fragmentation and spindle assembly defects

To analyze the consequences of accumulating STARD9-MD in mitosis, we used LAP-tagged STARD9-MD wild-type and serine-to-alanine mutant stable cell lines (expressing STARD9-MD from the same single chromosomal loci) to overexpress wild type and nonphosphorylatable/nondegradable STARD9-MD mutants and analyzed their mitotic defects by immunofluorescence microscopy. Consistent with our previous results, overexpressed STARD9-MD localized to the spindle poles and, to a lesser extent, the spindle microtubules

(Torres *et al.*, 2011; Figure 7A). However, the nonphosphorylatable/nondegradable S305A, S312A, and S317A mutants accumulated to very high levels at the spindle poles and spindle, consistent with our immunoblot analyses showing their stabilization in mitosis (Figure 7A). As a control, STARD9-MD with the S316A mutation that did not block STARD9-MD degradation remained at similar low levels as wild-type STARD9-MD (Figure 7A). Similarly, measurements of the total fluorescence intensity of LAP-STARD9-MD at the centrosome indicated that STARD9-MD protein levels were markedly increased in the S305A, S312A, and S317A mutants, whereas wild-type STARD9-MD and the degradation-competent S316A mutant remained low (Figure 7B). Also consistent with previous results, overexpression of STARD9-MD led to a modest but reproducible increase in the percentage of cells with spindle defects (PCM fragmentation and multipolar spindles): ~18% compared with ~8% control (Torres *et al.*, 2011; Figure 7, A and C). A similar effect was also seen with the degradation-competent S316A mutant (Figure 7, A and C). Of interest, overexpression of the nonphosphorylatable/nondegradable S305A, S312A, and S317A mutants led to significant increase in the percentage of cells with spindle assembly defects, ~25–30% (Figure 7, A and C). Consistently, live-cell time-lapse microscopy of nonphosphorylatable/nondegradable mutants like S317A indicated that overexpressing these mutants led to an arrest in mitosis, followed by apoptotic cell death (Figure 7D and Supplemental Movies S1–S4). These data indicated that posttranslational modification of STARD9-MD by Plk1 (phosphorylation) and SCFβ-TrCP (ubiquitination) was critical for controlling the levels of STARD9-MD at the centrosome during mitosis and that accumulation of STARD9-MD led to spindle assembly and cell division defects.

DISCUSSION

Mitotic kinases such as Plk1, Nek, Cdk1, and Aurora A/B are known to phosphorylate mitotic kinesins and thereby modulate their activities and functions during mitosis (Andrews *et al.*, 2004; Cahu *et al.*, 2008; Jang *et al.*, 2009; Bertran *et al.*, 2011; Sdelci *et al.*, 2011). An alternative mode of regulating kinesin activity/function is through protein degradation. The APC/C ubiquitin ligase targets numerous mitotic kinesins for degradation as the cells transition into anaphase, and degradation of these kinesins is critical for completion of mitosis (Funabiki and Murray, 2000; Gordon and Roof, 2001; Hildebrandt and Hoyt, 2001; Malcos and Cyr, 2011). On the other hand, the SCFβ-TrCP, another major ubiquitin ligase responsible for driving the cell cycle, degrades cell cycle regulators such as Emi1 and Bora in early mitosis (Margottin-Goguet *et al.*, 2003; Hansen *et al.*, 2004; Seki *et al.*, 2008b). However, the SCFβ-TrCP had not been demonstrated to degrade kinesins. Here we determined that the motor domain of the STARD9 mitotic kinesin is a substrate of the SCFβ-TrCP and a pool of STARD9-MD is degraded in mitosis. Our data suggest that in vivo the protein levels of full-length STARD9 could be regulated through Plk1 phosphorylation, SCFβ-TrCP ubiquitination, and proteasome-dependent degradation. Of interest, the STARD9-MD contained a highly conserved β-TrCP- binding motif, harbored putative Plk1 binding sites, and was phosphorylated by Plk1 and ubiquitinated by the SCFβ-TrCP during mitosis (Figures 1–6). In addition, a pool was degraded in a proteasome-dependent manner, and the remaining STARD9-MD remained localized to the centrosomes and mitotic spindle (Figure 7). The interactions that STARD9-MD maintains at the centrosome are unknown; it is likely, however, that its association with centrosomal components could protect it from Plk1 phosphorylation and/or SCFβ-TrCP ubiquitination. Thus it will be important to identify the full complement of STARD9-MD interactors and determine whether these factors protect STARD9-MD from posttranslational modifications.

Structural modeling of kinesin-3 family members indicates that L12 makes contact with the microtubule backbone. Of interest, STARD9 appears to be the only kinesin with a 26–amino acid insertion in L12, and within the context of our STARD9-MD studies, this insertion is heavily phosphorylated in mitosis. In addition to regulating STARD9-MD protein stability, phosphorylation could also affect the ability of STARD9-MD to interact with microtubules and/or hydrolyze ATP. Thus further structure–function analyses are necessary to fully understand how posttranslational modifications influence STARD9-MD's activity. Although Plk1 was shown to be important for phosphorylating STARD9-MD at serine 312, the identity of the kinase(s) required for phosphorylating other critical serines (305 and 317) that regulate STARD9-MD protein levels is unknown, as well as that of the kinase(s) that phosphorylate STARD9-MD at other serines (304, 307, 316, 319, 328, and 332) and threonine 321. Thus it will be important to identify the mitotic kinase(s) responsible for these phosphorylating events.

The composition of mammalian centrosomes and spindle assembly factors is more complex than that for lower eukaryotes. Consistently, factors critical for mammalian spindle assembly such as Bora, Kizuna, and STARD9 are not evolutionarily conserved (Oshimori *et al.*, 2006; Seki *et al.*, 2008b; Torres *et al.*, 2011). Mammalian cells have evolved specialized mechanisms to deal with an open mitosis and the stresses of forming a productive mitotic spindle. Not surprisingly, mammalian cells tightly regulate the protein levels of critical factors necessary for cell cycle progression. It is largely unknown why perturbing the levels of STARD9 has deleterious consequences (Torres *et al.*, 2011). One possibility is that STARD9 is in equilibrium with other PCM scaffolding factors, and the lack of complex formation in the absence of STARD9 or perturbation of these complexes through competition by overexpressing STARD9-MD may lead to complex inactivation. Further characterization of the interactions that STARD9 undergoes at the centrosome should provide insight into its mechanism of action.

MATERIALS AND METHODS

Cell culture and cell cycle synchronization

HeLa and HeLa Flp-In T-REx LAP-tagged stable cell lines were grown as described previously (Senese *et al.*, 2014). Cells were induced to express the indicated proteins by 0.1 μg/ml doxycycline (Sigma-Aldrich, St. Louis, MO) and synchronized in G1/S by treatment with 2 mM thymidine (Sigma-Aldrich) for 18-h. Alternatively, cells were synchronized at G2/M by a thymidine-nocodazole arrest (18 h in 2 mM thymidine-containing medium and then release into 330 nM nocodazole [Sigma-Aldrich]-containing medium for 12 h). To obtain synchronized cells in mitosis, cells were treated with 300 nM nocodazole (Sigma-Aldrich) for 12–20 h as indicated and collected by mitotic shake-off. To analyze the progression from mitosis to G1, after synchronization in early mitosis by nocodazole for 16 h, cells were collected by mitotic shake off, washed, and released into fresh medium. The proteasome inhibitor MG132 (Calbiochem, Billerica, MA) was added to mitotic-arrested cells at 10 μM 4 h before harvesting cells. For in vivo Plk1 inhibition, cells were incubated 200 nM GSK461364 (GlaxoSmithKline, Philadelphia, PA) or BI22536 (Selleckchem, Houston, TX). To determine the half-life of proteins, doxycycline-induced and mitotic- synchronized HeLa cells were released into the cell cycle and treated with 100 μg/ml cycloheximide (Sigma-Aldrich), and at the indicated time points, whole-cell extracts were prepared and subjected to immunoblot analysis with the indicated antibodies.

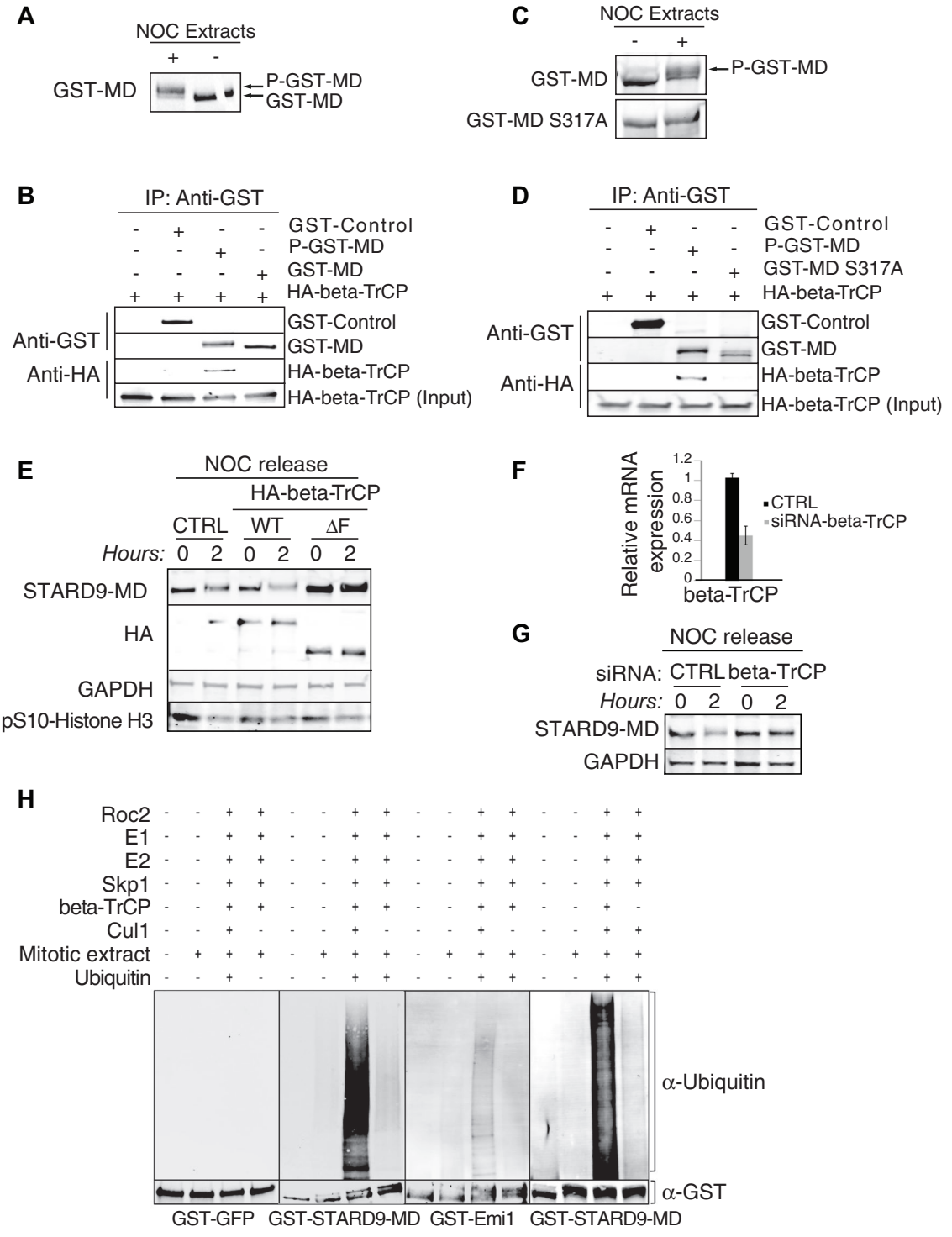

FIGURE 6: β-TrCP binds to STARD9-MD and regulates its degradation. (A) GST-STARD9-MD (GST-MD) was incubated with or without mitotic extracts and became phosphorylated in mitotic extracts. (B) β-TrCP binds to STARD9-MD in vitro. GST-STARD9-MD was incubated with HA-β-TrCP for 1 h and washed, and the binding was monitored by immunoblot analysis. (C) GST-STARD9-MD (GST-MD) or the mutant GST-STARD9-MD S317A (GST-MD S317A) was incubated with or without mitotic extracts, and only GST-MD became phosphorylated in mitotic extracts. (D) GST-STARD9-MD or GST-STARD9-MD S317A was incubated with HA-β -TrCP for 1 h and washed, and the binding was monitored by immunoblot analysis. (E) The LAP-tagged STARD9-MD wild-type cell line was transfected with HA-β-TrCP or HA-β-TrCPΔF overexpression vectors, synchronized in mitosis with nocodazole for 16 h, and released into the cell cycle, and the stability of STARD9-MD was monitored by immunoblot analysis. (F) The knockdown efficiency of siRNA targeting β-TrCP expression was determined by RT (reverse transcription)-qPCR. Data represent the average ± SD of three independent experiments. (G) The LAP-tagged STARD9-MD wild-type cell line was transfected with control siRNA or siRNA targeting β-TrCP, synchronized in mitosis with nocodazole for 16 h, and released into the cell cycle, and the stability of STARD9-MD was monitored by immunoblot analysis. (H) STARD9-MD is a substrate of the SCFβ-TrCP

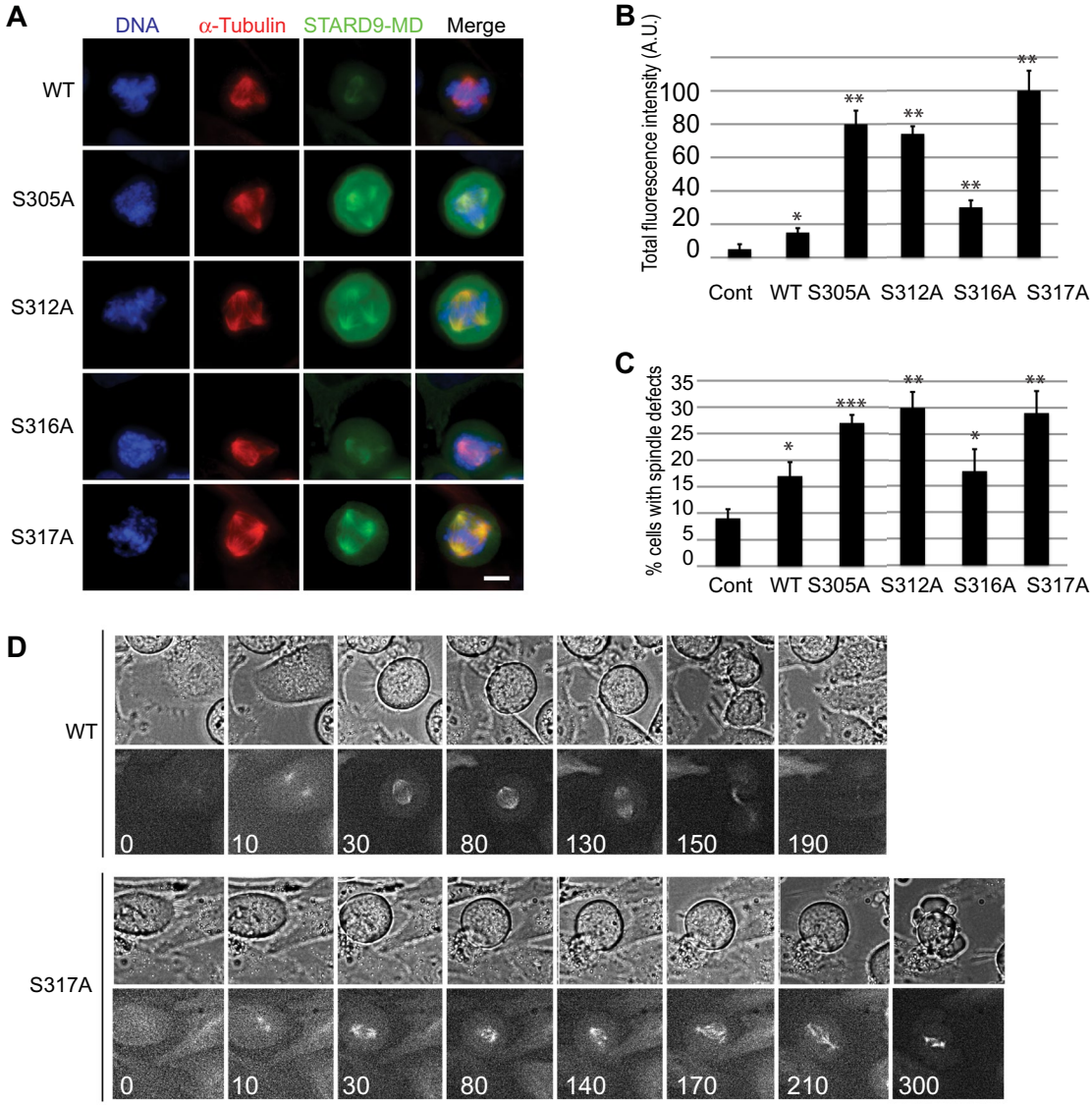

FIGURE 7: Increased levels of STARD9-MD lead to spindle assembly and cell division defects. (A) STARD9-MD wild-type and serine-to-alanine mutant stable cell lines were induced to express these proteins. Twenty hours postinduction, cells were fixed and stained for DNA, α-tubulin, and STARD9-MD and imaged by fluorescence microscopy. Bar, 5 μm. (B) Quantification of the fluorescence intensity signal from STARD9-MD wild-type and serine-to-alanine mutant proteins within a 3-μm radius surrounding the centrosome/spindle pole. Data represent the average ± SD of three independent experiments, 20 cells counted for each. *$p < 0.05$, **$p < 0.0005$. (C) The percentage of cells with spindle defects was quantified. Data represent the average ± SD of three independent experiments, 100 cells counted for each. *$p < 0.05$, **$p < 0.005$, ***$p < 0.0005$. (D) Live-cell time-lapse microscopy of STARD9-MD wild type and S317A mutant. Top, bright-field (BF) snapshots, and bottom, fluorescence (FL), of STARD-MD localization at the indicated time points in minutes. See Supplemental Movies S1–S4.

Plasmids, mutagenesis, and generation of stable cell lines

For STARD9-MD expression, the first 387 amino acids of STARD9 were fused to the C-terminus of either GST (pGEX-6P vector) or EGFP (pGLAP1 vector; Torres *et al.*, 2009). For expression in human cells, the pCS2-HA-β-TrCP, pCS2-HA-β-TrCPΔF, pCS2-HA-CUL1, pCS2-HA-PLK1, pCS2-HA-PLK1-K82R, and pCS2-HA-KATNA1 (control) vectors were used. In addition, the pGEX4T1-NT-EMI1 vector was used to express recombinant Emi1, and pDEST24-GST-GFP was used as an additional control. STARD9-MD point mutants were generated using the QuikChange Lightning Site-Directed Mutagenesis Kit (Agilent Technologies, La Jolla, CA) with primers carrying the desired mutations. All primers were purchased from Fisher Scientific (Pittsburgh, PA).

ubiquitin ligase. In vitro ubiquitination reactions were carried out with recombinant GST-STARD9-MD, GST-Emi1, or GST-GFP and with or without ubiquitin, E1, E2, Roc1, Skp1, Cul1, β-TrCP, and mitotic extracts. Products were resolved by SDS–PAGE and immunoblotted with anti-ubiquitin and anti-GST antibodies. Higher-molecular-weight bands are indicative of ubiquitination.

Primer sequences were as follows:

S304A STARD9-MD

Forward: 5′-ctgccagagcctcaacgcctcagtcagcaatggt-3′

Reverse: 5′-accattgctgactgaggcgttgaggctctggcag-3′

S305A STARD9-MD

Forward: 5′-cagagcctcaacagcgcagtcagcaatggtg-3′

Reverse: 5′-caccattgctgactgcgctgttgaggctctg-3′

S312A STARD9-MD

Forward: 5′-tcagcaatggtggtgacgctgggatccttagctctc-3′

Reverse: 5′-gagagctaaggatcccagcgtcaccaccattgctga-3′

S316A STARD9-MD

Forward: 5′-gtggtgacagtgggatccttgcctctccttctggg-3′

Reverse: 5′-cccagaaggagaggcaaggatcccactgtcaccac-3′

DM STARD9-MD

Forward: 5′-gtggtgacgctgggatccttgcctctccttctgggaccagc-3′

Reverse: 5′-gctggtcccagaaggagaggcaaggatcccagcgtcaccac-3′

S317A STARD9-MD

Forward: 5′-gtgggatccttagcgctccttctgggacc-3′

Reverse: 5′-ggtcccagaaggagcgctaaggatcccac-3′

TM STARD9-MD

Forward: 5′-ctgggatccttgccgctccttctgggacc-3′

Reverse: 5′-ggtcccagaaggagcggcaaggatcccag-3′

The pGLAP1-STARD9-MD wild-type and mutant vectors were used to generate doxycycline-inducible HeLa Flp-In T-REx LAP-STARD9-MD wild-type and mutant stable cell lines that express these fusion proteins from a specific single loci within the genome as described (Torres *et al.*, 2009).

Immunoprecipitation and LAP purification

Indicated cell lines or HeLa cells transfected with indicated vectors were arrested at the indicated cell cycle phases. Whole-cell extracts were prepared in LAP300 lysis buffer (50 mM 4-(2-hydroxyethyl)-1-piperazineethanesulfonic acid [HEPES], pH 7.4, 300 mM KCl, 1 mM ethylene glycol tetraacetic acid [EGTA], 1 mM $MgCl_2$, 10% glycerol) plus 0.3% NP-40, 0.5 mM dithiothreitol (DTT), 10 μM MG132, 20 mM *N*-ethylmaleimide (NEM), and protease and phosphatase inhibitor cocktail (Thermo Scientific, Waltham, MA). Immunoprecipitations were performed as previously described (Torres *et al.*, 2009). Samples were resolved in a 4–20% gradient Tris gel (Bio-Rad, Philadelphia, PA) with 3-(*N*-morpholino)propanesulfonic acid (MOPS) running buffer, transferred to polyvinylidene fluoride membrane, and immunoblotted with indicated antibodies. Similarly LAP-tag tandem affinity purifications were performed as described in (Torres *et al.*, 2009).

Recombinant protein expression and purification

Recombinant GST-fusion proteins (STARD9-MD wild type and mutants) were induced in *Escherichia coli* BL-21 pLyse-E with 300 μM isopropyl-β-D-thiogalactoside for 6 h at 30°C. After centrifugation, cells were lysed with lysis buffer (50 mM Tris-HCl, pH 7.4, 300 mM NaCl, 2.5 mM EDTA, 2.5 mM EGTA, 2 mM $MgCl_2$, 0.02% Triton X-100, 0.25 mM ATP, 1 mM DTT, and protease inhibitors). The lysate was passed through a microfluidizer and clarified by centrifugation at 15,000 rpm for 30 min. The binding to glutathione Sepharose beads (GE Healthcare) was performed for 2 h at 4°C. The pellet was washed in wash buffer (50 mM Tris-HCl, pH 7.4, 200 mM NaCl, 2.5 mM EDTA, 2.5 mM EGTA, 2 mM $MgCl_2$, 0.02% Triton X-100, 0.25 mM ATP, 1 mM DTT), and protein was eluted by adding elution buffer (50 mM Tris-HCl, pH 7.4, 200 mM NaCl, 2.5 mM EDTA, 2.5 mM EGTA, 2 mM $MgCl_2$, 0.02% Triton X-100, 10% glycerol, 0.25 mM ATP, 1 mM DTT, 50 mM glutathione). The purified protein was concentrated using an Amicon Ultra 30K concentrator and dialyzed in dialysis buffer (50 mM Tris-HCl, pH 7.4, 200 mM NaCl, 2.5 mM EDTA, 2.5 mM EGTA, 2 mM $MgCl_2$, 0.02% Triton X-100, 10% glycerol, 0.25 mM ATP, 1 mM DTT) overnight. The protein was concentrated again, aliquoted, and flash-frozen in liquid nitrogen and stored at −80°C.

Phosphorylation assays

Extracts of HeLa cells synchronized in G1/S by a thymidine treatment or in mitosis by a thymidine release into nocodazole treatment were prepared as described (Seki *et al.*, 2008a), aliquoted at a concentration of 10 μg/μl, flash-frozen in liquid nitrogen, and stored at −80°C. For each reaction on ice, 10 μl of extracts was supplemented with 1 μl of ATP regeneration solution (Enzo Life Science, Farmingdale, NY), and 1 μg of bacterial STARD9-MD protein was added. Reactions were shifted to 30°C and stopped at the indicated times by the addition of sample buffer. Samples were resolved by a 4–20% gradient Tris gel (Bio-Rad) with MOPS running buffer.

Phosphatase assays

Cells were lysed in LAP300 lysis buffer (50 mM HEPES, pH 7.4, 300 mM KCl, 1 mM EGTA, 1 mM $MgCl_2$, 10% glycerol) plus 0.3% NP-40, 0.5 mM DTT, 10 μM MG132, 20 mM NEM, and protease inhibitor cocktail (Thermo Scientific), and 1200 U of λ phosphatase (New England BioLabs, Ipswich, MA) was added to 50 μg of protein lysates. The reaction was carried out at 30°C for 1 h and stopped by the addition of sample buffer.

Ubiquitination reactions

A 10-μg amount of recombinant GST-tagged STARD9-MD, EMI1, or GFP was bound to magnetic glutathione beads (Thermo Scientific) and incubated with mitotic HeLa cell extracts along with an ATP regeneration system (Enzo Life Sciences) for 3 h at 30°C. After 3 h, a master mix containing all the ubiquitination components (ubiquitin [Enzo Life Sciences], ROC1, E1, E2, Skp1, with or without β-TrCP, with or without CUL1, in a buffer containing 20 mM HEPES, 5 mM NaCl, 5 mM $MgCl_2$, DTT, MG132, and protease and phosphatase inhibitor cocktail (Thermo Scientific) and ATP regeneration system was added to the tubes and further incubated for 90 min at 30°C. The beads were then washed four times with a wash buffer containing 20 mM HEPES, 100 mM NaCl, 5 mM $MgCl_2$, 15 mM imidazole, 0.5% Triton-X, β-mercaptoethanol, DTT, MG132, and a protease and phosphatase inhibitor cocktail. The beads were then boiled in 2× Laemmli sample buffer (Bio-Rad) and loaded onto a 4–12% TGX gel (Bio-Rad), followed by Western transfer. The blots were subsequently probed with anti-GST (Abcam, Cambridge, MA) and anti-ubiquitin (Enzo Life Sciences) antibodies.

Homology modeling of the STARD9 motor domain structure

The STARD9 motor domain structure was modeled using the modeller-9v8 program by satisfying spatial constraints (Sali and Blundell, 1993). Briefly, the STARD9 sequence was blasted against the PDB database in the National Center for Biotechnology Information server to retrieve homologous sequences with solved three-dimensional structures. KIF1A (PDB ID 1IA0) was identified as the best template, which shares 48% sequence identity with the STARD9 kinesin motor. The initial sequence alignment was performed using the automodel routine as part of the automated modeling procedures. One hundred structures were generated by varying the initial conformation and were subsequently refined using simulated annealing and molecular

dynamics simulation. To identify the best model, each refined structure was scored using Discrete Optimized Protein Energy (DOPE), and the top five models (B99990019, B99990044, B99990051, B99990058, and B99990090) were rescored using ERRAT potential by analyzing the statistics of nonbonded interactions (Colovos and Yeates, 1993; Shen and Sali, 2006). The best model (B99990019) was selected based on the combined assessment of statistical scores and geometric evaluation by the PROCHECK and VERIFY3D programs within the Structural Analysis and Verification (SAVES) server (Luthy *et al.*, 1992; Laskowski *et al.*, 1993). Model evaluation with Ramachandran plot shows that the final model has 92.1% residues in the most favorable region, 7.6% residues in the additional allowed region, and 0% residues in the disallowed region. VERIFY3D results show that 88% of the residues had an average 3D-1D score >0.2, indicating that the model is reasonable. The final STARD9 kinesin homology model was structurally aligned with the KIF1A template and visualized using the molecular modeling software Chimera (Pettersen *et al.*, 2004). STARD9-MD shows strong structure similarity to KIF1A-MD. In particular, the ATPase catalytic site is highly conserved. Of interest, STARD9 contains an extended loop 12 with a 26–amino acid insertion; this loop is flexible and may play a role in protein–protein interactions and posttranslational modification.

Molecular modeling of the β-TrCP–STARD9-MD phosphodegron interaction

To model the β-TrCP–STARD9-MD interaction, the STARD9-MD degron (DpSGILSpS) was structurally aligned with the β-TrCP substrate β-catenin within the WD40 domain (PDB 1P22:A.C). To further optimize the STARD9-MD degron binding, the complex was subsequently energy minimized, followed by a 100-ps molecular dynamics simulation using the MOE software. The final peptide conformation was consistent with that previously reported for a nontypical degron. Specifically, the two phosphorylated serines pS312 and pS317 were anchored on two sides of the substrate-binding site through multiple hydrogen bonds and electrostatic interactions with residues Ser-325, Ser-309, Arg-285, and Ty-r271 and Arg-431, Gly-408, and Arg-410, respectively. The hydrogen bonds formed between S316 and Ser448 were specific for the STARD9-MD degron, whereas that between D311, Arg-521, and Tyr-488 were conserved among most β-TrCP substrate degrons (Kanarek *et al.*, 2010). Note that Leu-315 was inserted further into the inner groove through hydrophobic interactions with residue Arg-474, causing loop bending.

STARD9 motor domain phosphorylation site mapping by liquid chromatography–tandem mass spectrometry

The LAP-STARD9-MD (wild type) cell line was grown in roller bottles, induced with 0.1 μg/ml doxycycline, and simultaneously arrested in mitosis as described (Torres *et al.*, 2009). Cells were harvested by mitotic shake-off and lysed in the presence of protease (Roche, Branford, CT), phosphatase (Pierce, Rockford, IL), deubiquitinase (NEM; Enzo Lifesciences), and proteasome inhibitors (MG132; Enzo Lifesciences). LAP-STARD9-MD was purified from extracts using our tandem affinity purification protocol (Torres *et al.*, 2009). Eluates were resolved on a 4–12% SDS–PAGE, and gel slices corresponding to the phosphorylated form of the STARD9-MD (and an adjacent control region) were excised and collected in a 1.5-ml tube, washed twice with 50% acetonitrile, flash frozen, and stored until examination by mass spectrometry. Mass spectrometry–based proteomic analysis of STARD9-MD and phosphorylation site mapping (ST: +79.9663Da) was performed at the Harvard Mass Spectrometry and Proteomics Resource Laboratory by microcapillary reverse-phase HPLC nano–electrospray tandem mass spectrometry on a Thermo LTQ-Orbitrap mass spectrometer as described (Vanderwerf *et al.*, 2009). Identified phosphorylation sites are indicated in Supplemental Figure S4.

Antibodies

Immunofluorescence, immunoblotting, and immunoprecipitations were carried out using antibodies against the following: GFP and Securin (Abcam), phospho-S10-H3 (Millipore, Billerica, MA), glyceraldehyde-3-phosphate dehydrogenase (GeneTex, Irvine, CA), ubiquitin (Enzo Life Sciences), GST (Abcam), CDC27 (GeneTex), Wee1 (GeneTex), S-tag (GeneTex), α-tubulin (Serotec, Raleigh, NC), HA (Cell Signaling, Danvers, MA), cyclin A and cyclin B (Santa Cruz Biotechnology, Dallas, TX), and Plk1 (Abcam). Secondary antibodies conjugated to fluorescein isothiocyanate (FITC) and Cy3 were from Jackson ImmunoResearch (Affinipure, West Grove, PA).

siRNA-based gene expression knockdown

Cells were transfected with 50 nM Dharmacon ON-TARGETplus SMARTpool siRNA targeting PLK1 (L-003290-00) or β-TRCP (L-003463-00) using Lipofectamine 3000 (Invitrogen, Grand Island, NY) according to the manufacturer's protocol. At 48 h posttransfection, cells were collected, and whole extracts were subjected to immunoblot analysis with the indicated antibodies.

Real-time PCR

For β-TrCP knockdown validation, RNA was isolated using PureLink RNA Mini Kit (Ambion, Grand Island, NY) and used as template for synthesis of cDNA using SuperScript II Reverse Transcriptase. The cDNA was subsequently used as template for quantitative RT-PCR analysis performed on an Applied Biosystems 7500 Fast Real-Time PCR System using the SYBR Green PCR kit as indicated by the manufacturer (Applied Biosystems). The amount of mRNA was normalized to Rpl32 mRNA, a housekeeping control gene. Samples were analyzed for gene expression using the following primers: β-TrCP forward, 5′-ATCGGATTCCACGGTCAGAG-3′, and reverse, 5′-CTCTGACCGTGGAATCCGAT-3′; Rpl32, forward, 5′-AAGCGAAACTGGCGGAAAC-3′, and reverse, 5′-TAACCGATGTTGGGCATCAG -3′.

Immunofluorescence and live-cell time-lapse microscopy

Immunofluorescence microscopy was carried out essentially as described in Torres *et al.* (2010).

HeLa stable cell lines were induced to express STARD9-MD wild type and serine-to- alanine mutants for 24 h, fixed with 4% paraformaldehyde, permeabilized with 0.2% Triton X-100/phosphate-buffered saline, and costained with 0.5 μg/ml Hoechst 33342 and indicated antibodies. Images were captured with a Leica DMI6000 microscope (Leica DFC360 FX Camera, 63×/1.40–0.60 numerical aperture [NA] oil objective, Leica AF6000 software) at room temperature using Hoechst 3342 and secondary FITC and Cy3 antibodies (Jackson ImmunoResearch, West Grove, PA). Images were deconvolved with Leica Application Suite 3D Deconvolution software and exported as TIFF files. For fluorescence intensity measurements, a 3-μm circle surrounding the centrosome/spindle pole was drawn, and the total fluorescence intensity was measured using Leica AF6000 software. Data represent the average ± SD of three independent experiments, with 20 cells counted for each. The highest average intensity (for the S317A cell line) was set to 100 and used to normalize the other intensity measurements. For quantifying spindle defects, 100 cells from three independent experiments for each cell line were counted, and the data are presented as the average ± SD. For time-lapse microscopy, LAP-STARD9-MD (wild-type and S317A mutant) cells were concurrently induced with doxycycline to express fused proteins and arrested with 2 mM thymidine for 18 h, washed, and

released into fresh media. Cells were imaged live 5 h postrelease for 10 h using the same Leica DMI6000 microscope as described at 37°C and 5% CO_2 using a 40×/0.75 NA air objective. To ensure good resolution of the entire cell, *Z*-stacks were captured every 1 µm for 10 µm at 40× magnification, and stacks were deconvolved using Leica 3D deconvolution software and compressed as maximum intensity projection images. Images were converted to movies using QuickTime software (Apple). Each frame represents a 10-min interval.

ACKNOWLEDGMENTS

We thank William Sullivan for Plk1 protein. J.T. was supported by an American Cancer Society Research Scholar Grant. This material is based on work supported by the National Science Foundation under Grant MCB1243645 to J.Z.T., and any opinions, findings, and conclusions or recommendations expressed are those of the authors and do not necessarily reflect the views of the National Science Foundation. K.C. was supported by a Whitcome Predoctoral Fellowship.

REFERENCES

Andrews PD, Ovechkina Y, Morrice N, Wagenbach M, Duncan K, Wordeman L, Swedlow JR (2004). Aurora B regulates MCAK at the mitotic centromere. Dev Cell 6, 253–268.

Barford D (2011). Structure, function and mechanism of the anaphase promoting complex (APC/C). Q Rev Biophys 44, 153–190.

Barr FA, Sillje HH, Nigg EA (2004). Polo-like kinases and the orchestration of cell division. Nat Rev Mol Cell Biol 5, 429–440.

Bertran MT, Sdelci S, Regue L, Avruch J, Caelles C, Roig J (2011). Nek9 is a Plk1-activated kinase that controls early centrosome separation through Nek6/7 and Eg5. EMBO J 30, 2634–2647.

Budde PP, Kumagai A, Dunphy WG, Heald R (2001). Regulation of Op18 during spindle assembly in Xenopus egg extracts. J Cell Biol 153, 149–158.

Busino L, Donzelli M, Chiesa M, Guardavaccaro D, Ganoth D, Dorrello NV, Hershko A, Pagano M, Draetta GF (2003). Degradation of Cdc25A by beta-TrCP during S phase and in response to DNA damage. Nature 426, 87–91.

Cahu J, Olichon A, Hentrich C, Schek H, Drinjakovic J, Zhang C, Doherty-Kirby A, Lajoie G, Surrey T (2008). Phosphorylation by Cdk1 increases the binding of Eg5 to microtubules in vitro and in Xenopus egg extract spindles. PLoS One 3, e3936.

Cardozo T, Pagano M (2004). The SCF ubiquitin ligase: insights into a molecular machine. Nat Rev Mol Cell Biol 5, 739–751.

Casenghi M, Meraldi P, Weinhart U, Duncan PI, Korner R, Nigg EA (2003). Polo-like kinase 1 regulates Nlp, a centrosome protein involved in microtubule nucleation. Dev Cell 5, 113–125.

Colovos C, Yeates TO (1993). Verification of protein structures: patterns of nonbonded atomic interactions. Protein Sci 2, 1511–1519.

Elia AE, Cantley LC, Yaffe MB (2003). Proteomic screen finds pSer/pThr-binding domain localizing Plk1 to mitotic substrates. Science 299, 1228–1231.

Frescas D, Pagano M (2008). Deregulated proteolysis by the F-box proteins SKP2 and beta-TrCP: tipping the scales of cancer. Nat Rev Cancer 8, 438–449.

Funabiki H, Murray AW (2000). The Xenopus chromokinesin Xkid is essential for metaphase chromosome alignment and must be degraded to allow anaphase chromosome movement. Cell 102, 411–424.

Gordon DM, Roof DM (2001). Degradation of the kinesin Kip1p at anaphase onset is mediated by the anaphase-promoting complex and Cdc20p. Proc Natl Acad Sci USA 98, 12515–12520.

Hansen DV, Loktev AV, Ban KH, Jackson PK (2004). Plk1 regulates activation of the anaphase promoting complex by phosphorylating and triggering SCFbetaTrCP-dependent destruction of the APC Inhibitor Emi1. Mol Biol Cell 15, 5623–5634.

Hildebrandt ER, Hoyt MA (2001). Cell cycle-dependent degradation of the Saccharomyces cerevisiae spindle motor Cin8p requires APC(Cdh1) and a bipartite destruction sequence. Mol Biol Cell 12, 3402–3416.

Jang CY, Coppinger JA, Seki A, Yates JR 3rd, Fang G (2009). Plk1 and Aurora A regulate the depolymerase activity and the cellular localization of Kif2a. J Cell Sci 122, 1334–1341.

Kanarek N, London N, Schueler-Furman O, Ben-Neriah Y (2010). Ubiquitination and degradation of the inhibitors of NF-kappaB. Cold Spring Harb Perspect Biol 2, a000166.

Laney JD, Hochstrasser M (2011). Analysis of protein ubiquitination. Curr Protoc Protein Sci Chapter 14, Unit 14.15.

Lang V, Janzen J, Fischer GZ, Soneji Y, Beinke S, Salmeron A, Allen H, Hay RT, Ben-Neriah Y, Ley SC (2003). betaTrCP-mediated proteolysis of NF-kappaB1 p105 requires phosphorylation of p105 serines 927 and 932. Mol Cell Biol 23, 402–413.

Laskowski RA, Moss DS, Thornton JM (1993). Main-chain bond lengths and bond angles in protein structures. J Mol Biol 231, 1049–1067.

Lee K, Rhee K (2011). PLK1 phosphorylation of pericentrin initiates centrosome maturation at the onset of mitosis. J Cell Biol 195, 1093–1101.

Lowery DM, Clauser KR, Hjerrild M, Lim D, Alexander J, Kishi K, Ong SE, Gammeltoft S, Carr SA, Yaffe MB (2007). Proteomic screen defines the Polo-box domain interactome and identifies Rock2 as a Plk1 substrate. EMBO J 26, 2262–2273.

Luthy R, Bowie JU, Eisenberg D (1992). Assessment of protein models with three-dimensional profiles. Nature 356, 83–85.

Mailand N, Bekker-Jensen S, Bartek J, Lukas J (2006). Destruction of Claspin by SCFbetaTrCP restrains Chk1 activation and facilitates recovery from genotoxic stress. Mol Cell 23, 307–318.

Malcos JL, Cyr RJ (2011). An ungrouped plant kinesin accumulates at the preprophase band in a cell cycle-dependent manner. Cytoskeleton (Hoboken) 68, 247–258.

Margottin F, Bour SP, Durand H, Selig L, Benichou S, Richard V, Thomas D, Strebel K, Benarous R (1998). A novel human WD protein, h-beta TrCp, that interacts with HIV-1 Vpu connects CD4 to the ER degradation pathway through an F-box motif. Mol Cell 1, 565–574.

Margottin-Goguet F, Hsu JY, Loktev A, Hsieh HM, Reimann JD, Jackson PK (2003). Prophase destruction of Emi1 by the SCF(betaTrCP/Slimb) ubiquitin ligase activates the anaphase promoting complex to allow progression beyond prometaphase. Dev Cell 4, 813–826.

Oshimori N, Ohsugi M, Yamamoto T (2006). The Plk1 target Kizuna stabilizes mitotic centrosomes to ensure spindle bipolarity. Nat Cell Biol 8, 1095–1101.

Pettersen EF, Goddard TD, Huang CC, Couch GS, Greenblatt DM, Meng EC, Ferrin TE (2004). UCSF Chimera–a visualization system for exploratory research and analysis. J Comput Chem 25, 1605–1612.

Ramachandran GN, Ramakrishnan C, Sasisekharan V (1963). Stereochemistry of polypeptide chain configurations. J Mol Biol 7, 95–99.

Rath O, Kozielski F (2012). Kinesins and cancer. Nat Rev Cancer 12, 527–539.

Sali A, Blundell TL (1993). Comparative protein modelling by satisfaction of spatial restraints. J Mol Biol 234, 779–815.

Sdelci S, Bertran MT, Roig J (2011). Nek9, Nek6, Nek7 and the separation of centrosomes. Cell Cycle 10, 3816–3817.

Seki A, Coppinger JA, Du H, Jang CY, Yates JR 3rd, Fang G (2008a). Plk1- and beta-TrCP-dependent degradation of Bora controls mitotic progression. J Cell Biol 181, 65–78.

Seki A, Coppinger JA, Jang CY, Yates JR, Fang G (2008b). Bora and the kinase Aurora a cooperatively activate the kinase Plk1 and control mitotic entry. Science 320, 1655–1658.

Senese S, Lo YC, Huang D, Zangle TA, Gholkar AA, Robert L, Homet B, Ribas A, Summers MK, Teitell MA, *et al.* (2014). Chemical dissection of the cell cycle: probes for cell biology and anti-cancer drug development. Cell Death Dis 5, e1462.

Shen MY, Sali A (2006). Statistical potential for assessment and prediction of protein structures. Protein Sci 15, 2507–2524.

Torres JZ (2012). STARD9/Kif16a is a novel mitotic kinesin and antimitotic target. Bioarchitecture 2, 19–22.

Torres JZ, Ban KH, Jackson PK (2010). A specific form of phospho protein phosphatase 2 regulates anaphase-promoting complex/cyclosome association with spindle poles. Mol Biol Cell 21, 897–904.

Torres JZ, Miller JJ, Jackson PK (2009). High-throughput generation of tagged stable cell lines for proteomic analysis. Proteomics 9, 2888–2891.

Torres JZ, Summers MK, Peterson D, Brauer MJ, Lee J, Senese S, Gholkar AA, Lo YC, Lei X, Jung K, *et al.* (2011). The STARD9/Kif16a kinesin associates with mitotic microtubules and regulates spindle pole assembly. Cell 147, 1309–1323.

Vanderwerf SM, Svahn J, Olson S, Rathbun RK, Harrington C, Yates J, Keeble W, Anderson DC, Anur P, Pereira NF, *et al.* (2009). TLR8-dependent TNF-(alpha) overexpression in Fanconi anemia group C cells. Blood 114, 5290–5298.

Verhey KJ, Hammond JW (2009). Traffic control: regulation of kinesin motors. Nat Rev Mol Cell Biol 10, 765–777.

Winston JT, Strack P, Beer-Romero P, Chu CY, Elledge SJ, Harper JW (1999). The SCFbeta-TRCP-ubiquitin ligase complex associates specifically with phosphorylated destruction motifs in IkappaBalpha and beta-catenin and stimulates IkappaBalpha ubiquitination in vitro. Genes Dev 13, 270–283.

Zhang L, Shao H, Huang Y, Yan F, Chu Y, Hou H, Zhu M, Fu C, Aikhionbare F, Fang G, *et al.* (2011). PLK1 phosphorylates mitotic centromere-associated kinesin and promotes its depolymerase activity. J Biol Chem 286, 3033–3046.